

The overview of the ATLAS local hadronic calibration.

Guennadi Pospelov, for the ATLAS hadronic calibration group.

Max-Planck-Institut für Physik, Werner-Heisenberg-Institut
Föhringer Ring 6, 80805 Munich, Germany

E-mail: pospelov@mppmu.mpg.de

Abstract.

We present the concept of the local hadronic calibration for the ATLAS calorimeter system as a tool to get calibrated jets at particle level for any jet algorithm. The procedure is based on detailed **Geant4** simulations providing information on energy deposits in all parts of the ATLAS detector. Calibration starts from topological clusters reconstructed and calibrated at the electromagnetic scale. First classification step tags clusters as mainly electromagnetic, or hadronic depending on cluster shape variables. Clusters which are identified as being electromagnetic are kept at the electromagnetic scale. Hadronic clusters receive cell weights to correct for the invisible energy deposits of hadrons. Next steps are out-of-cluster corrections for lost energy deposited in calorimeter cells outside of reconstructed clusters and dead material corrections for energy deposited outside of active calorimeter volumes. Finally out-of-jet corrections are applied to get the final jet energy scale.

1. Introduction

The jet energy scale is one of the main systematic uncertainties in many physics studies foreseen with the ATLAS detector [1]. Top mass reconstruction or measurements of inclusive jet cross-section are examples relevant for the first data taking phase. The initial parton energy differs from the energy of the hadronic shower because of detector effects, like calorimeter non-compensation and energy losses in dead material, jet effects, like bending of secondary particles out of the jet cone by the magnetic field or jet reconstruction algorithm specifics, and effects from the collision physics environment.

In this paper we present the concept of the local hadronic calibration for jets to the particle level independent on any jet algorithm. The ultimate goal of the procedure is to provide jet algorithms with constituents — calibrated clusters with energies corresponding to the stable particle energies. The key feature of the approach is to factorize corrections in several sequential steps to disentangle detector effects of different types and to correct them independently.

Starting point for the local hadronic calibration is topological clustering [2] in the calorimeter cells which have been calibrated at the electromagnetic (*em*) scale. Cluster shape variables are then used to classify clusters as having electromagnetic or hadronic nature. The hadron-like clusters are subject of a cell weighting procedure to compensate for the lower response of the calorimeter to hadronic deposits, while clusters classified as electromagnetic-like, are kept at the original scale. Next out-of-cluster (OOC) corrections for lost energy deposited in calorimeter cells outside of reconstructed clusters in the tail of hadronic shower are applied. Finally, dead material

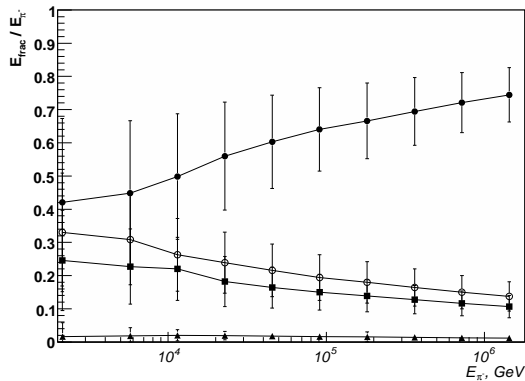


Figure 1. Calibration energy fractions (\bullet - visible *em*, \circ - visible *non-em*, \blacksquare - invisible, \blacktriangle - escaped) released in active and inactive material in the endcap region ($1.5 < |\eta| < 3.0$) by single charged pions vs. the pion energy.

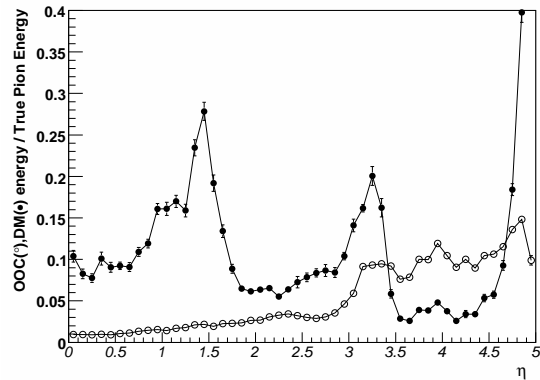


Figure 2. Fractions of true calibration hit energies outside topological clusters but inside the calorimeters (\circ) and outside calorimeters (\bullet) as function of pion pseudorapidity for 200 GeV pion energy.

(DM) corrections are applied on the cluster level to account for energy deposits outside of active calorimeter volumes, e.g. in the cryostat, the magnetic coil and calorimeter intermodular cracks.

To derive the correction coefficients for all calibration steps we use actual energy deposits in active and inactive volumes known from detailed *Geant4* [3] simulations via the so-called *calibration hits* mechanism.

2. Simulation and Calibration Hits

The classification and calibration methods described in this paper are based on detailed simulations of single pions in the standard ATLAS environment. The data set consist of 10^6 neutral and $2 \cdot 10^6$ charged pions with initial η, ϕ coordinates randomly distributed across the entire detector. The initial pion energies were generated in 1000 logarithmically equidistant steps from 150 MeV to 2 TeV.

Calibration hits provide access to the energy deposits in active (liquid argon, scintillator), inactive (absorber) and dead material regions for the following four categories of energy deposits:

- visible *em*-energy: The energy released by electrons or positrons via ionization.
- visible *non-em*-energy: The energy released by charged particles other than electrons or positrons via ionization.
- in-visible energy: The energy released by non-ionizing processes such as break-up of nuclear bindings.
- escaped energy: The energy leaving the mother volume in form of non-interacting or escaping particles like neutrinos or muons.

Figure 1 shows the average fraction of each of these 4 categories summed over the active and inactive regions in the endcap calorimeters as a function of the pion energy. Error bars on the figure represent *rms* values. Figure 2 shows the total out-of-cluster and dead material energy fractions known from calibration hits as function of pion pseudorapidity for 200 GeV charged pions.

The aim of the calibration is to reconstruct the lost invisible and escaped energy on an event-by-event basis with measured energy depositions inside calorimeter cells.

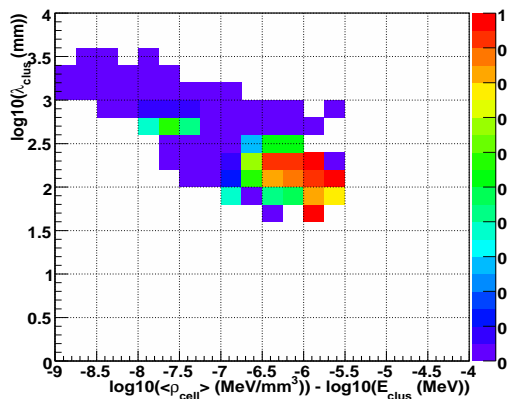


Figure 3. Probability weights to observe a neutral pion cluster for $8 \text{ GeV} < E_{\text{cluster}} < 16 \text{ GeV}$.

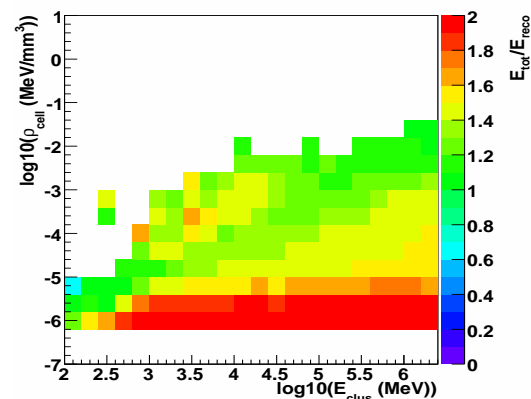


Figure 4. Hadronic cell weights for Tile barrel sampling 1 at $0.2 < |\eta| < 0.4$.

3. Local Hadronic Calibration

3.1. Cluster Classification

Aim of the cluster classification is to distinguish between clusters seeded by electromagnetic or hadronic interactions. For topological clusters where the correspondence of cluster and particle level is close this would lead to a separation of electrons, photons and neutral pions on one side from charged hadrons (mainly pions) and neutrons on the other side such that both particle classes can be optimally calibrated.

The current default procedure in ATLAS is to classify topological clusters basing on the predicted phase-space population of clusters stemming from charged and neutral pion simulations. The separation of hadronic from electromagnetic showers relies on the following cluster shape variables: the average cell energy density $\langle \rho \rangle$ and the depth of the shower center λ_{center} . For both particle species the 4-dimensional phase space for clusters in $|\eta|$, E_{cluster} , $\log_{10}(\lambda_{\text{center}})$ and $\log_{10}(\langle \rho \rangle) - \log_{10}(E_{\text{cluster}})$ is binned and filled with simulated pions in the energy range $E_{\text{cluster}} = 200 \text{ MeV} - 2 \text{ TeV}$ and $|\eta| < 5$. Assuming an a-priori probability ratio of 1 : 2 for observing a neutral pion over a charged pion the probability weight in each phase-space bin for observing a neutral pion is given by: $w_i = n_i^{\pi^0} / (n_i^{\pi^0} + 2n_i^{\pi^{\pm}})$, where $n_i^{\pi^{0,\pm}}$ is the fraction of clusters at given energy and η of neutral or charged pions in a given phase-space bin i from the simulation. A cluster is classified as electromagnetic if the lookup value for $w_i > 0.5$ at a given cluster phase-space bin.

Figure 3 shows the classification weights obtained with this procedure for the region $0.2 < |\eta| < 0.4$ and $8 \text{ GeV} < E_{\text{cluster}} < 16 \text{ GeV}$ on a colored scale from 0 (purely hadronic) to 1 (purely electromagnetic) as a function of the two moments $\langle \rho \rangle$ and λ_{center} . It is clearly visible that electromagnetic showers dominate the region of high energy density and small cluster depth. It is also apparent from the plots that classification is most difficult for clusters with smaller energies as the distributions for charged and neutral pions have larger overlaps in that regime.

The classification performance in terms of the energy fractions classified as electromagnetic and hadronic for neutral and charged single pions is shown in figure 5. For neutral pions the method reaches classification efficiencies of 80 – 85% above 50 GeV, but below that energy the electromagnetic fraction drops linearly with the logarithm of the pion energy. For charged pions the hadronic fraction is rather stable between 80 – 90% over the entire energy range – at low energies due to the low classification efficiency of neutral pions and at large energies due to the better separation of neutral and charged showers.

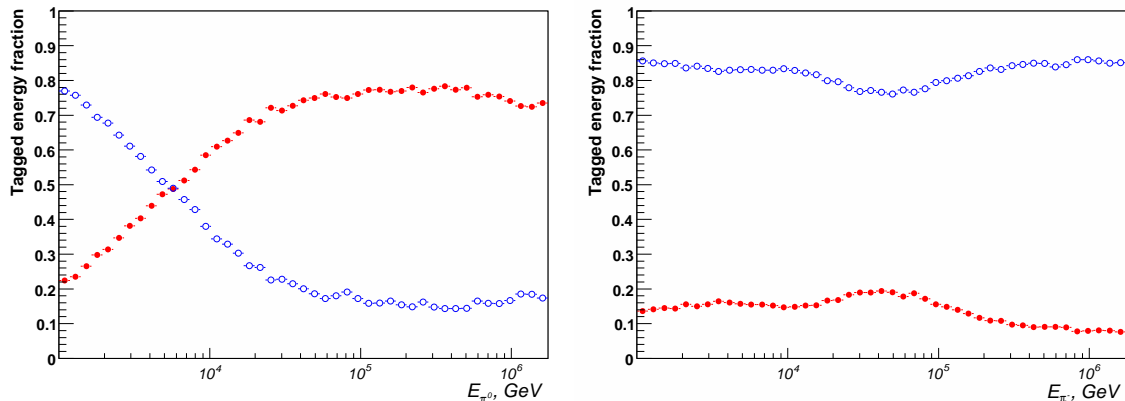


Figure 5. Energy fractions of single pions classified as electromagnetic (●) or hadronic (○) for π^0 's (left), π^\pm 's (right) as function of the pion energy averaged over all η and ϕ .

3.2. Cluster Weighting

For clusters classified as hadronic a H1-type cell-based weighting procedure [4, 5] is applied to correct for invisible and escaped energy fractions. The weight tables are filled with the ratios $E_{\text{cell}}^{\text{calib}}/E_{\text{cell}}^{\text{reco}}$, where $E_{\text{cell}}^{\text{reco}}$ is the regular simulated energy based on the visible energy in the active media including noise, while $E_{\text{cell}}^{\text{calib}}$ is the sum of the four calibration energies deposited in the given cells active and inactive parts. Average weights are kept as a function of the cluster energy the cell belongs to, the energy density $\rho_{\text{cell}} = E_{\text{cell}}^{\text{reco}}/V_{\text{cell}}$ of the cell, and the $|\eta|$ of the cell center. There are 25 equidistant $|\eta|$ -bins from 0.0 to 5.0, 20 logarithmic energy-density bins from $-7 < \log_{10}(\rho_{\text{cell}}(\text{MeV}/\text{mm}^3)) < 1$ and 22 logarithmic cluster energy bins from $\log_{10}(100(\text{MeV})) < \log_{10}(E_{\text{clus}}(\text{MeV})) < \log_{10}(2 \cdot 10^6(\text{MeV}))$. Examples of the actual weights for the first sampling of the Tile calorimeter obtained this way from $2 \cdot 10^6$ charged pions are shown in figure 4.

3.3. Out-of-Cluster corrections

Out-of-cluster corrections aim for recovering from the lost low energetic deposits at the tails of hadronic showers. This energy is deposited in calorimeter cells which are not part of any reconstructed cluster due to noise thresholds in the clustering.

The total fraction of out-of-cluster energy from single pion simulations w.r.t. the weighted total energy inside clusters is averaged in bins of pion energy, pion $|\eta|$, and the pion depth λ in the calorimeter. The λ values of all clusters in a given event are combined with energy proportional weights to obtain the latter. 12 energy bins with the boundaries $\{0, 1, 2, 4, 8, 16, 32, 64, 128, 256, 512, 1024, 2048\}$ GeV, 25 equidistant $|\eta|$ bins from 0 to 5 and 20 equidistant bins in $\log_{10}(\lambda/\text{mm})$ from 0 to 4 define the lookup table.

However, out-of-cluster energy estimated with the help of tables of that kind turned out to be overrated in multi particle event. This is due to the fact, that energy which is outside of one cluster could actually be inside the other cluster. To resolve this problem the level of isolation of clusters is used [6]. It is determined by the fraction of cells on its outer perimeter not included in other clusters. An isolation of 0 means that all cells on its outer perimeter are included in neighboring clusters, a value of 1 indicates that the cluster is totally isolated – i.e. that all its neighbor cells are not part of any cluster. This isolation fraction is multiplied with the expected out-of-cluster energy fraction for each cluster as obtained from the out-of-cluster tables described above. This accounts for the fact that clusters tend to be less isolated in full events compared to single pion events from simulations or beam tests.

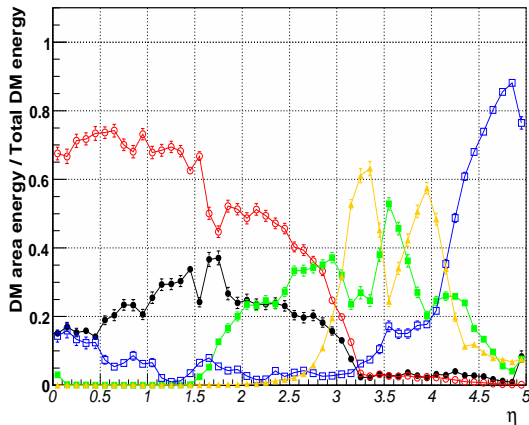


Figure 6. Ratio of energy deposited in different DM regions (\bullet - before *em* calorimeter, \circ - between *em* and *had*, \blacksquare - intermodular cracks, \square - leakages, \blacktriangle - before forward calorimeter) to the total DM energy for charged pion with energy 200 GeV.

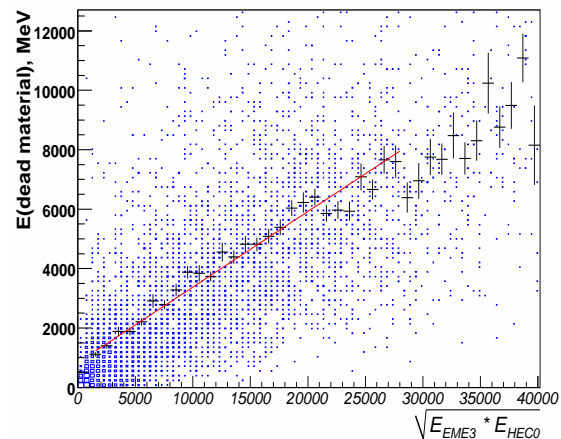


Figure 7. Dependence of energy deposited between *em* and *had* endcap calorimeters on $\sqrt{E_{EME3} \cdot E_{HEC0}}$, where E_{EME3} energy in last *em* sampling, E_{HAD0} energy in first *had* samplings.

3.4. Dead material corrections

Dead material corrections are accounting for energy deposited outside of active zones of the electromagnetic and hadronic calorimeters. This includes energy deposited in upstream material (Inner Detector material, magnetic coil, cryostat walls), different crack regions between calorimeter modules and material behind calorimeter system (leakages). Figure 6 shows the ratio of energy deposited in different DM regions to the total DM energy for charged pions with 200 GeV energy as a function of the pion pseudorapidity. These regions are treated variously to get and to apply DM correction coefficients. For upstream material the good correlations of DM deposits with the preshower signals are used. Deposits between electromagnetic and hadronic calorimeters are corrected for by weighting the geometric average of signals in the last *em* and first *had* sampling. (see figure 7). Correction coefficients then are parametrised as a function of cluster energy and pseudorapidity. For intricate DM regions where there are no cluster quantities correlating well with DM energy deposits, 3 dimensional lookup tables on $E_{cluster}$, $\eta_{cluster}$, $\lambda_{cluster}$ are used to store average ratios of DM energy to the cluster energy.

4. Performance

Figure 8 shows the ratio of reconstructed over simulated pion energy at the *em*-scale, and after applying 3 sequential steps of local hadronic calibration: hadronic weighting, out-of-cluster and dead material corrections. The plot has been obtained for 100 GeV single charged pions in the region $0.2 < |\eta| < 0.4$. It is clearly seen that each step shifts the mean of the reconstructed energy toward the truth energy and, at the end, gives the correct value. The energy resolution is improving on each step as well.

The performance of local hadronic calibration on di-jet events is presented in figure 9. Jets are formed by the K_T jet algorithm with $R = 0.6$ from topological clusters, calibrated with the local hadronic calibration scheme, and compared to the truth matched jets. Thus, for the barrel and endcap regions the local hadronic calibration recovers linearity for 100 GeV jets up to 92%, while for 10 GeV jets missed energy reaches 25%. Main sources of remaining energy correction and their impact on the energy underestimation are presented below (calculation has been done

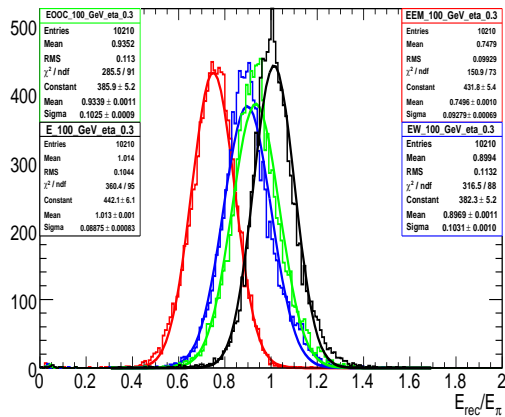


Figure 8. The ratio of reconstructed over simulated pion energy at various stages of the calibration.

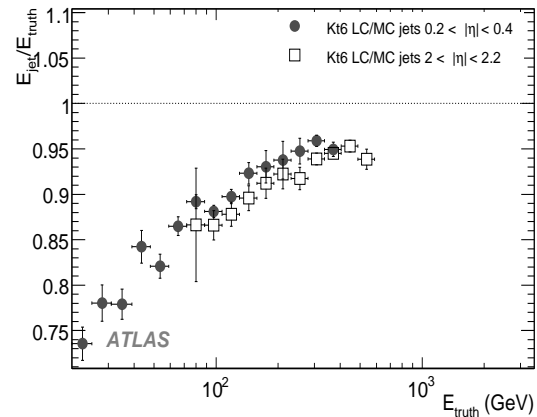


Figure 9. Linearity for K_T jet algorithm with $R = 0.6$ for 2 different η regions as a function of jet energy.

for $p_{\perp} \simeq 150\text{GeV}$):

- missclassification (hadronic deposits are treated as electromagnetic and vice versa) - 3%.
- calorimeter inefficiency (particle leaves signal below noise threshold) - 3%.
- lost particles (bending of particles outside the acceptance cone by magnetic field) - 2%.

All these effects are subject of jet level corrections which are currently under development.

5. Conclusion

In this article the local hadron calibration as a tool to calibrate topological clusters from em scale to the particle level is discussed. It will be used to provide jet correction for the ATLAS detector. The method includes four consecutive steps. In a first step clusters are classified as electromagnetic or hadronic based on cluster energy density and calorimeter cluster depth. In the second step hadronic-like clusters are corrected for the invisible energy released in hadronic interactions. Then energy deposited in calorimeter cells not belonging to any cluster and in dead material outside calorimeter is corrected for. The correction coefficients are derived from single neutral and charged pion simulations. After application of the last calibration steps, the method is able to improve energy resolution and to restore true energy for single pions. For jets reconstruction the method is proven to recover linearity up to 92% in di-jet events with $p_{\perp} \simeq 150\text{GeV}$. The main sources of remaining missing energy are: missclassification, calorimeter inefficiency for low energetic pions and bending of particles out of the jet cone. They are the subject of the very last jet level correction step, which is currently under development.

References

- [1] ATLAS Collaboration 2008 The ATLAS experiment at the CERN Large Hadron Collider *submitted to JINST* 06/05/2008
- [2] Lampl W *et al* 2008 Calorimeter clustering algorithms: Description and Performance *ATLAS Note ATL-LARG-PUB-2008-002*
- [3] Agostinelli S *et al* 2003 GEANT4 — a simulation toolkit *Nucl. Instr. and Meth. A* **506** 250-303
- [4] H1 Collaboration 1994 *Nucl. Instr. and Meth. A* 344 (1994) 492
- [5] H.P. Wellisch, J.P. Kubenka, H. Oberlack, P. Schacht 1994 *Preprint MPI-PhE/94-03*
- [6] Bergeas E *et al* 2008 Topological cluster classification and weighting *ATLAS Note ATL-COM-LARG-2008-006*